Supporting Information

A high capacity $V_4C_3T_z$ MXene electrode: expanding the limits of stable electrochemical windows using a highly concentrated LiBr/H_2O electrolyte

Beatriz Mendoza-Sánchez,[*,†,⊥] Enrique Samperio-Niembro,[†] Atharva H. Ladole,[†,‡] Liuda Mereacre,[†] Michael Knapp,[†] Camille Douard,[¶,§] Thierry Brousse,[¶,§] and Christopher E. Shuck[‖]

†*Institute for Applied Materials-Energy Storage Systems (IAM-ESS), Karlsruhe Institute of Technology, Eggenstein-Leopoldshafen, D-76344, Germany*

‡*Institute for Energy and Materials Processes-Reactive Fluids, University of Duisburg-Essen, Duisburg,47057, Germany*

¶*Nantes Université, CNRS, Institut des Matériaux de Nantes Jean Rouxel, IMN, 2 rue de la Houssinière BP32229, 44322 Nantes cedex 3, France*

§*Réseau sur le Stockage Electrochimique de l'Energie (RS2E), CNRS FR 3459, F-80039, France*

‖*Department of Chemistry and Chemical Biology, Rutgers University, 123 Bevier Road, Piscataway, NJ 08854, USA*

⊥*Corresponding author*

E-mail: beatriz.sanchez.wa@gmail.com

Contents

S1 XRD structural data

The following table reports on the structural data of the Rietveld refinement of V_4AlC_3 powders. For a full report on derivation and analysis, see our previous work.[1]

Table S1: Structural parameters of phases in V_4AlC_3. Numbers in brackets give statistical deviations for the digit to the left. Standard deviations have been multiplied by the Bérar factor to correct for local correlations. The profile R-factor $R_p = 4.08$, the weight profile R-factor $R_{wp} = 5.5$ and $\chi^2 = 6.53$. Reprinted from,[1] Copyright (2024), with permission from Elsevier.

Phase	**Space group /(source)**	**a** (Å)	**b** (Å)	**c** (Å)	$\alpha = \beta$ (°)	γ(°)	**wt.**%
V_4AlC_3	P 6_3/m m c	2.92795(6)	2.92795(6)	22.7116(5)	90	120	91.85(0.51)
VC	F m -3 m (ICSD 22263)	4.1622(3)6	4.1622(3)6	4.1622(3)6	90	90	2.55(0.17)
V_6C_5	P 31 1 2 (ICSD 71098)	5.083(1)16	5.083(1)16	14.471(5)49	90	120	1.48(0.03)
V_2O_5	P m n 21 (ICSD 1011126)	11.36(7)953	4.35(2)314	3.59(2)738	90	90	3.13(0.37)
Al_2O_3	R -3 c (ICSD 9770)	4.760(3)86	4.760(3)86	12.98(2)990	90	120	0.99(0.18)

S2 Preliminary molecular dynamics studies of $LiBr/H_2O$ electrolytes

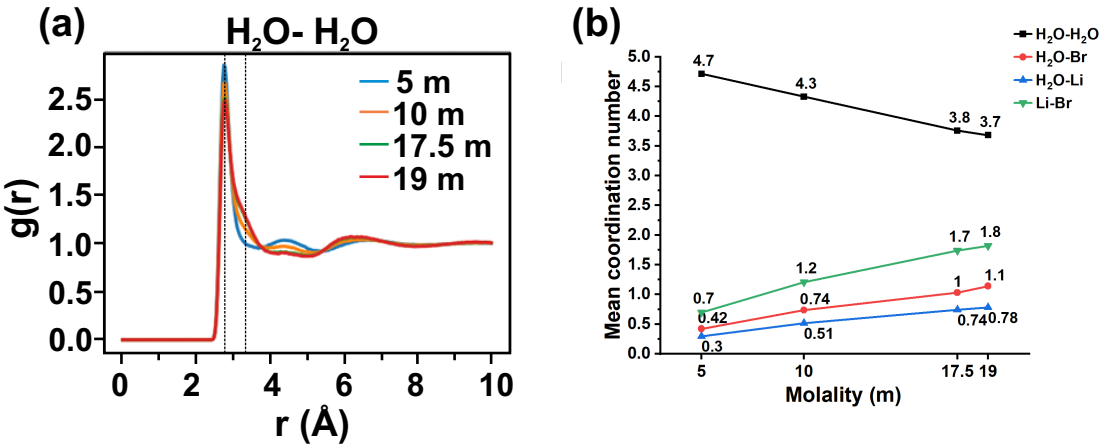

Figure S1: Molecular dynamics studies of 5 m, 10 m, 17.5 m and 19 m $LiBr/H_2O$ electrolytes. Derived (a) radial distribution functions of water-water interactions - dashed lines indicate peaks at 2.8 $\AA$ and 3.4 $\AA$ -, and (b) coordination numbers of ion-ion and ion-water interactions as function of molality.

S3 Electrochemical window selection data

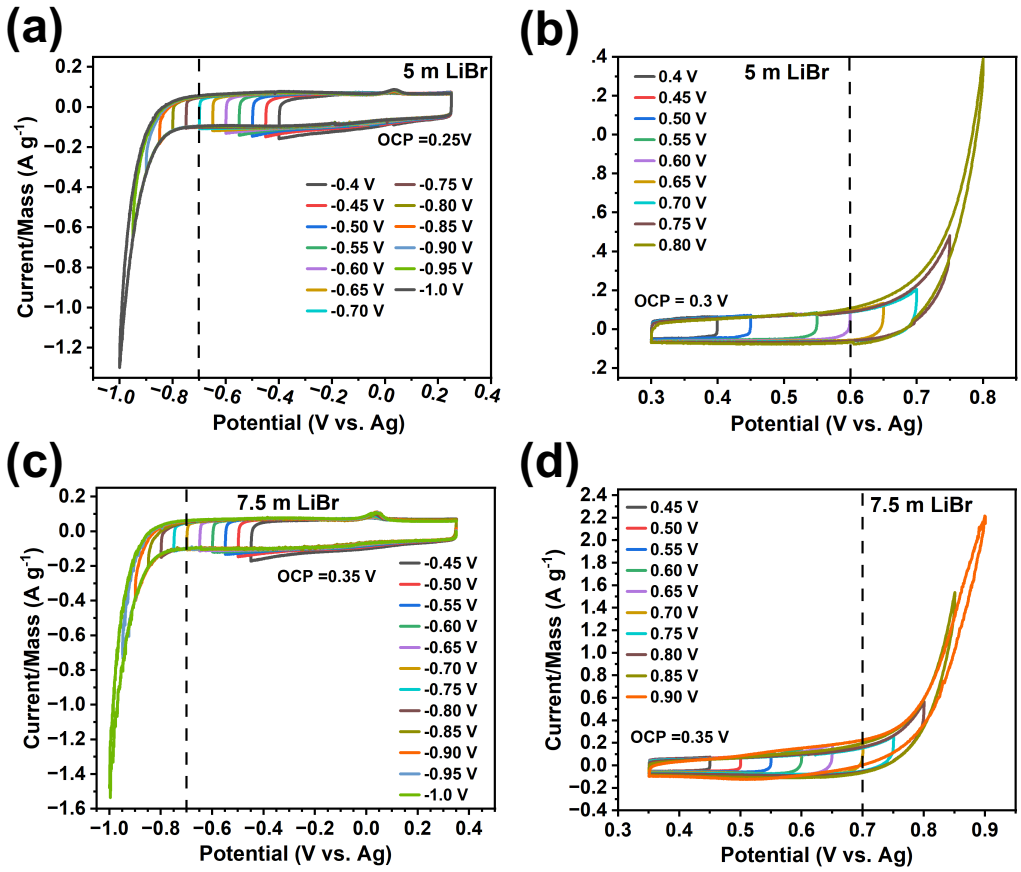

Figure S2: Window selection studies in (a),(b) 5 m and (c),(d) 7.5 m LiBr. (a)-(d) Cyclic voltammograms at a 0.5 mV s^{-1} scan rate from the open circuit potential (OCP) to (a),(c) negative potentials and (b),(d) positive potentials. The dashed lines indicate the stability limits of the electrochemical windows (see main text).

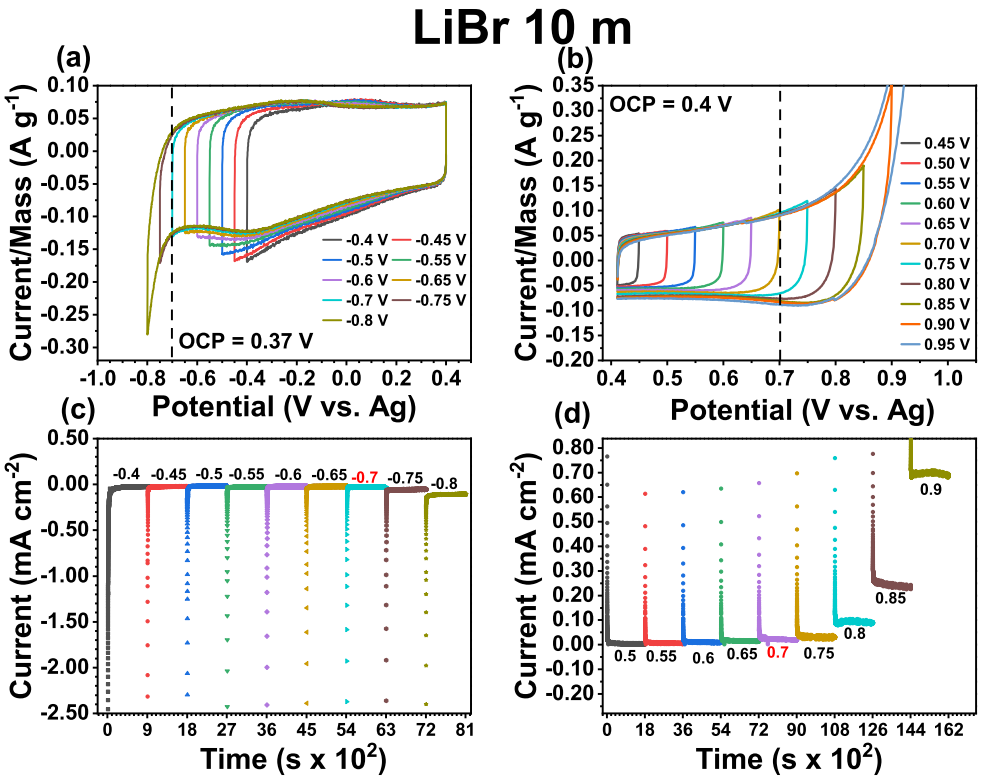

Figure S3: Window selection studies in 10 m LiBr. (a),(b) Cyclic voltammograms at a 0.5 mV s^{-1} scan rate from the open circuit potential (OCP) to (a) negative potentials and (b) positive potentials, (c),(d) chronoamperograms performed at the indicated constant potentials (V) for 15-30 min. The dashed lines indicate the stability limits of the electrochemical windows (see main text).

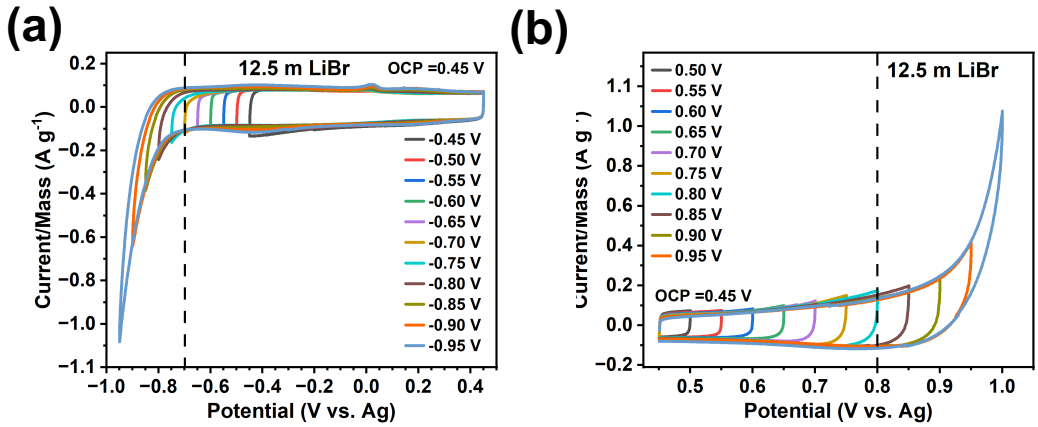

Figure S4: Window selection studies in 12.5 m LiBr. Cyclic voltammograms at a 0.5 mV s^{-1} scan rate from the open circuit potential (OCP) to (a) negative potentials and (b) positive potentials.The dashed lines indicate the stability limits of the electrochemical windows (see main text). The dashed lines indicate the stability limits of the electrochemical windows (see main text).

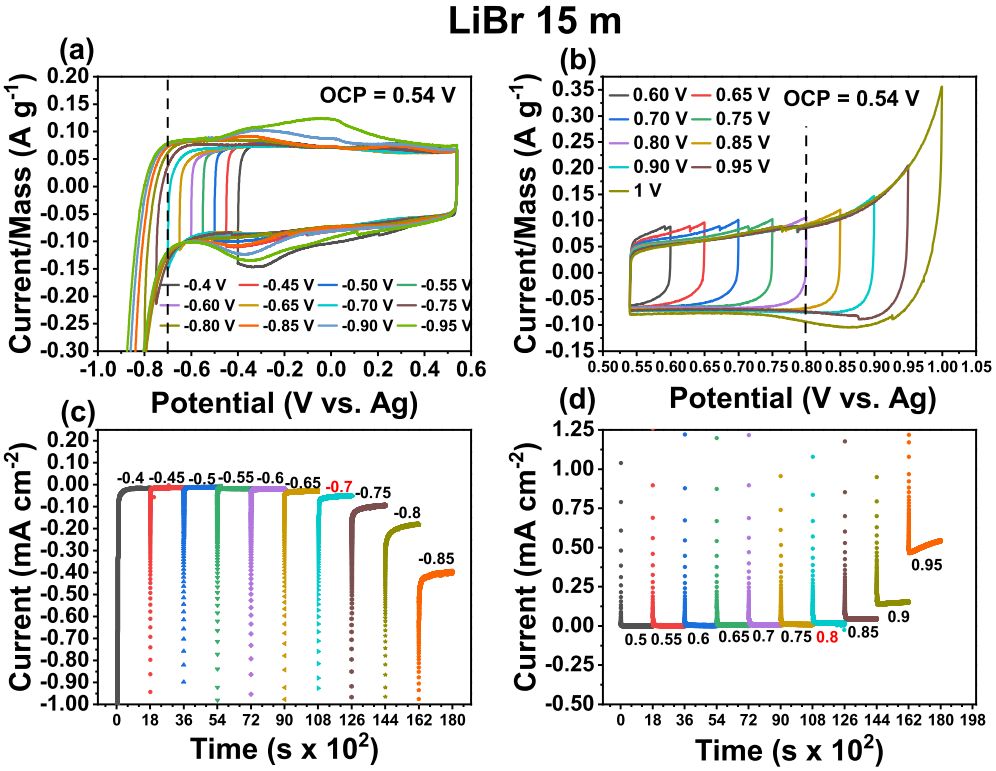

Figure S5: Window selection studies in 15 m LiBr. (a),(b) Cyclic voltammograms at a 0.5 mV s^{-1} scan rate from the open circuit potential (OCP) to (a) negative potentials and (b) positive potentials, (c),(d) chronoamperograms performed at the indicated constant potentials (V) for 15-30 min. The dashed lines indicate the stability limits of the electrochemical windows (see main text).

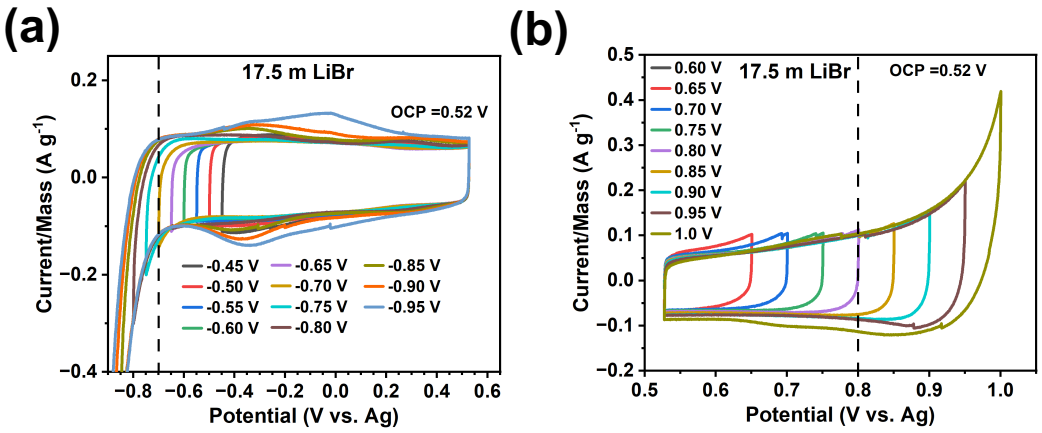

Figure S6: Window selection studies in 17.5 m LiBr. Cyclic voltammograms at a 0.5 mV s^{-1} scan rate from the open circuit potential (OCP) to (a) negative potentials and (b) positive potentials. The dashed lines indicate the stability limits of the electrochemical windows (see main text).

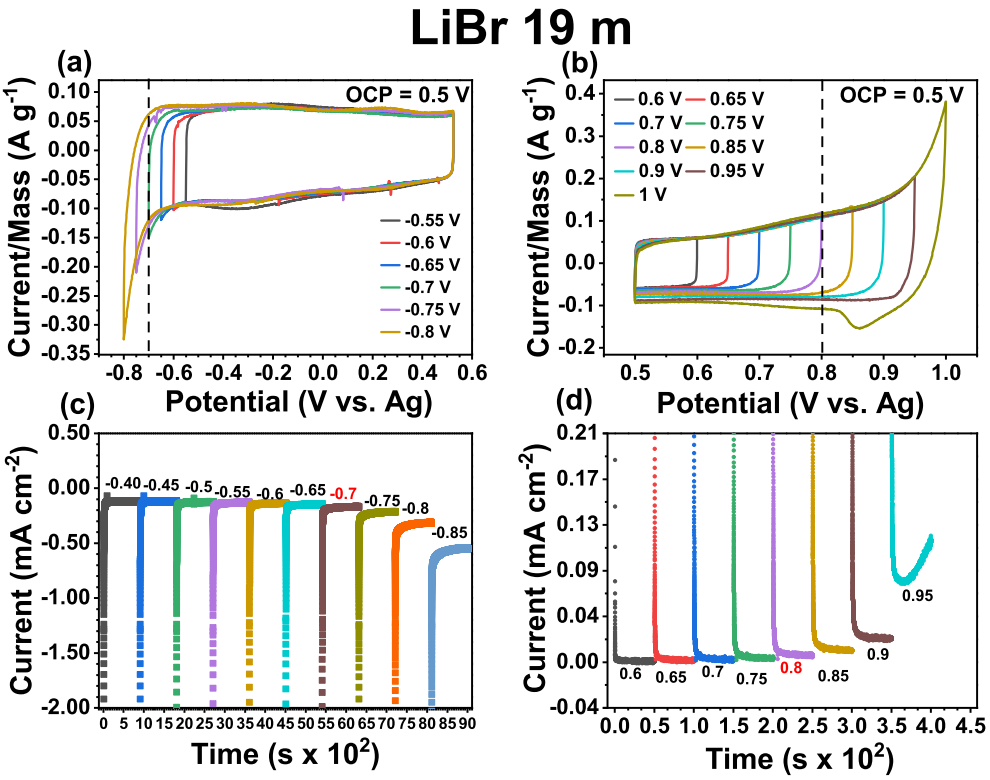

Figure S7: Window selection studies in 19 m LiBr. (a),(b) Cyclic voltammograms at a 0.5 mV s^{-1} scan rate from the open circuit potential (OCP) to (a) negative potentials and (b) positive potentials, (c),(d) chronoamperograms performed at the indicated constant potentials (V) for 15-30 min. The dashed lines indicate the stability limits of the electrochemical windows (see main text).

S4 Further cyclic voltammetry data of $V_4C_3T_z$ electrodes

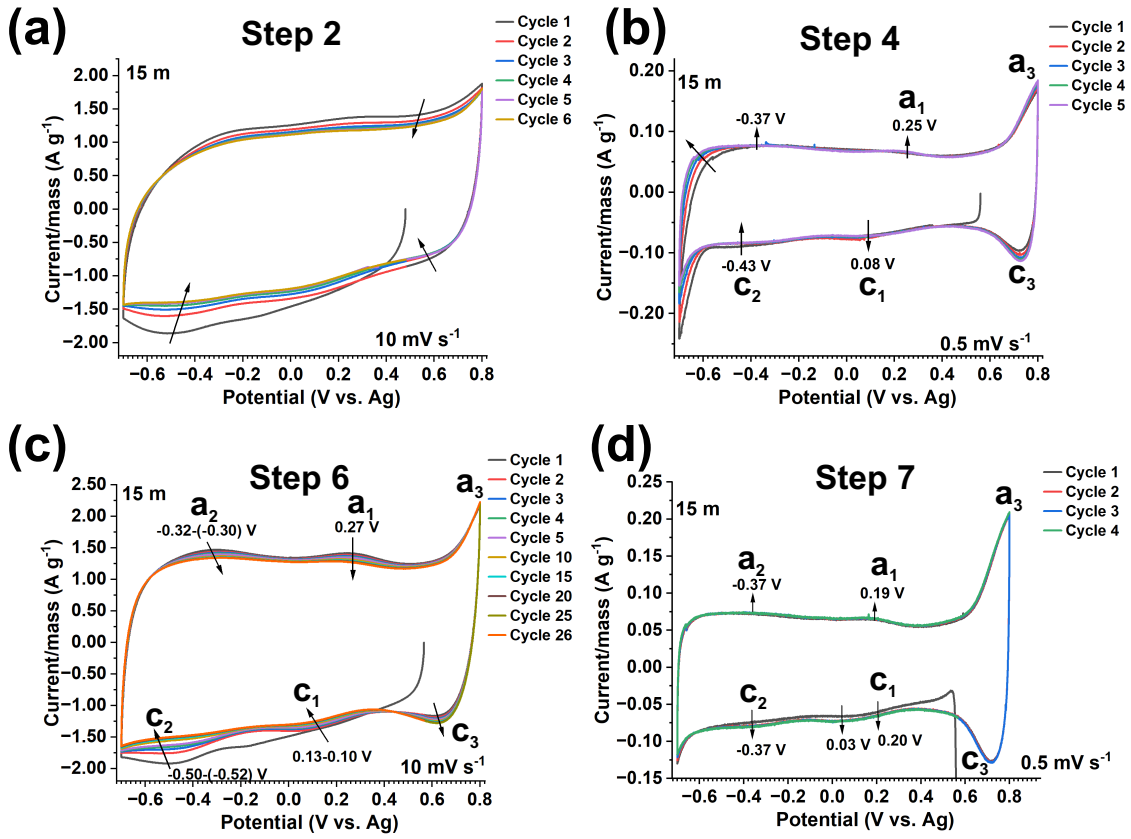

Figure S8: Cyclic voltammetry (CV) tests of $V_4C_3T_z$ film electrodes in a 15 m LiBr electrolyte, a half cell set up and a -0.7 to 0.8 V vs. Ag electrochemical window. (a) CV at 10 mV s^{-1} (step 2), (b) CV at 0.5 mV s^{-1} (step 4), (c) CV at 10 mV s^{-1} (step 6) and (d) CV at 0.5 mV s^{-1} (step 7). The arrows indicate currents at specified potentials or potential ranges from cycle 1 to cycle n.

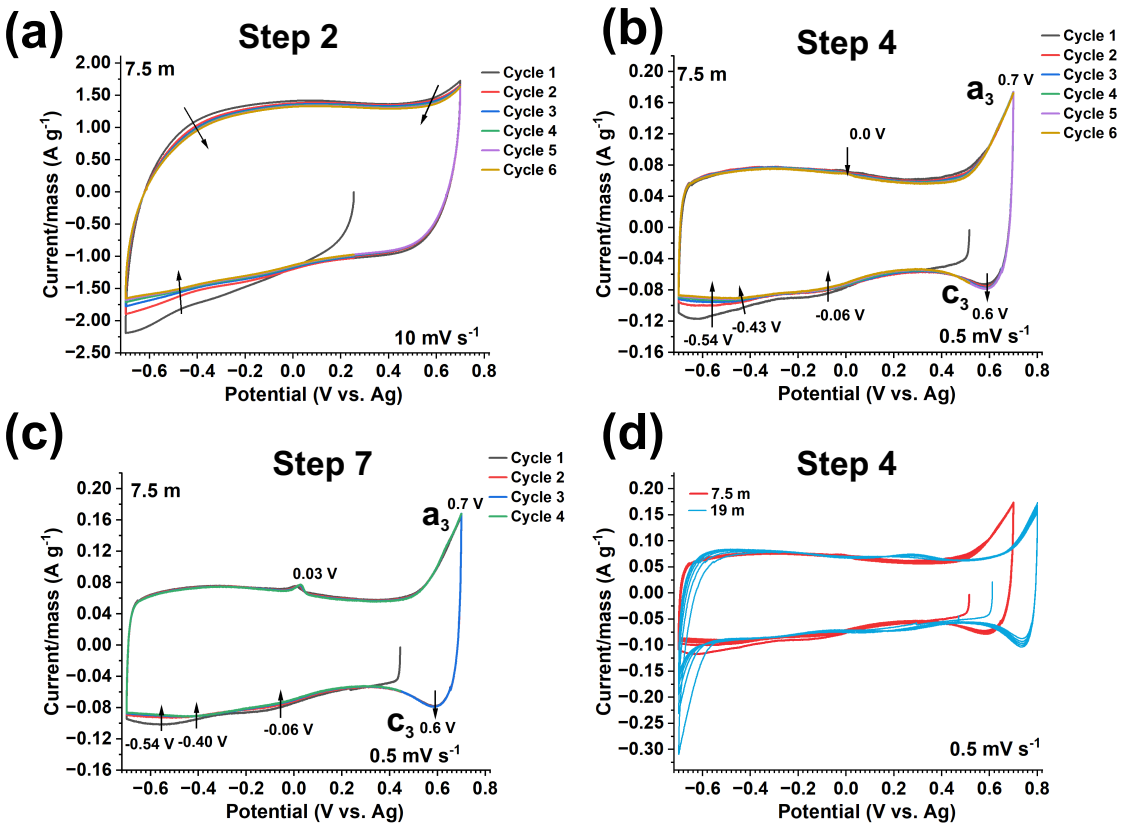

Figure S9: CV tests of $V_4C_3T_z$ film electrodes in a 7.5 m LiBr electrolyte, a half cell set up and a -0.7 to 0.7 V vs. Ag electrochemical window. (a) CV at 10 mV s^{-1} (step 2), (b) CV at 0.5 mV s^{-1} (step 4), (c) CV at 0.5 mV s^{-1} (step 7) and (d) CV at 0.5 mV s^{-1} (step 4) in 7.5 m and 19 m LiBr electrolytes. The arrows indicate currents at specified potentials or potential ranges from cycle 1 to cycle n. No activation was performed in this electrode (10 mV s^{-1} for 25 cycles, step 6).

S5 Cyclic voltammetry data of glassy carbon

Glassy carbon was used a current collector for all tests performed in this work. In order to test the electrochemical activity of the glassy carbon itself in the LiBr electrolyte, CV tests were performed in a half cell set up using either a beaker-type cell or a Swagelok cell. In the beaker-type cell, a glassy carbon rod (6 mm diameter) was used as working electrode, a graphite rod was used as counter electrode and an Ag wire was used as reference electrode. This configuration was preferred to enhance the surface area of the current collector in contact with the electrolyte. In the Swagelok cell, two glassy carbon rods (where the glassy carbon area in contact with the electrolyte is a disc of 3 mm diameter) were used as current collectors, separated by approximately 1 mm, and an Ag wire was used as reference electrode.

A CV test was performed in the beaker-type cell, using 5 m LiBr electrolyte, in a -1 to 1 V vs. Ag electrochemical window (EW) and at 10 mV s^{-1} (Figure S10a). The CV shows a pronounced oxidation/reduction activity at 1 V, indicating OER or oxidation/reduction processes related to the Br^{-1} anion. This activity was enhanced in the 6 mm rod glassy carbon due to the larger surface area as compared to the disc area of 3 mm diameter used in the Swagelok cell. In addition, an anodic current peak was present at -0.11 V vs. Ag, which can be better visualized in the inset in Figure S10b. This is the current peak that was observed in CV tests of $V_4C_3T_z$ film electrodes in 5 m, 7.5 m and 10 m LiBr electrolytes (main text, Figure 4b). Here, a CV of a test of a $V_4C_3T_z$ film electrode, in the same electrolyte and in a standard Swagelok cell, was added in the same graph to appreciate that this current peak had its origin in the glassy carbon-electrolyte interface (Figure S10b).

Similar CV tests were performed in 15 m LiBr for both, the glassy carbon current collector and the $V_4C_3T_z$ film electrode (both in Swagelok cells) (Figure S10c). For the latter, the CV test was performed for 5,000 cycles. Over the cycles, the current peak moved from -0.04 V to 0.05 V vs. Ag, which is just at the same potential than the anodic peak of the glassy carbon. This confirmed the origin of this electrochemical activity at the glassy carbon-electrolyte interface. The shift towards positive potentials and the growing magnitude of

the current peak over cycling for the CV test of the $V_4C_3T_z$ film is most likely linked to an increased contact of the electrolyte with the glassy carbon current collector resulting from minor mechanical changes induced by cycling.

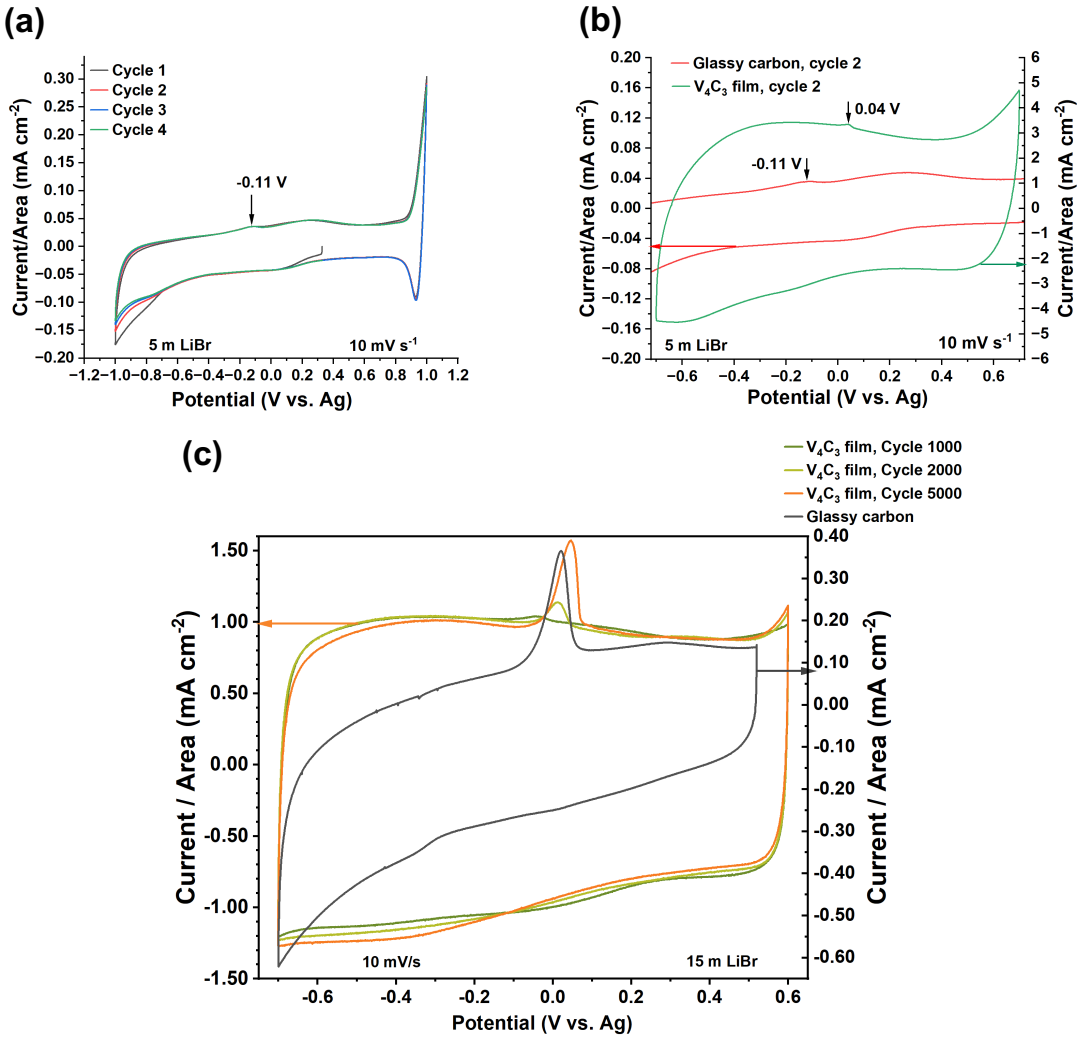

Figure S10: CV tests of glassy carbon current collectors in half cell set ups described in the text. (a) CV in 5 m LiBr performed at 10 mV s^{-1} (beaker-type cell), (b) a corresponding inset and a CV of a $V_4C_3T_z$ film electrode performed in a Swagelok cell in 5 m LiBr electrolyte at 10 mV s^{-1}, and (c) CV tests of the glassy current collector (Swagelok cell) and a $V_4C_3T_z$ film electrode (Swagelok cell) in 15 m LiBr, performed at 10 mV s^{-1}. Potentials of interest are indicated by arrows and text.

S6 Capacitive tendency

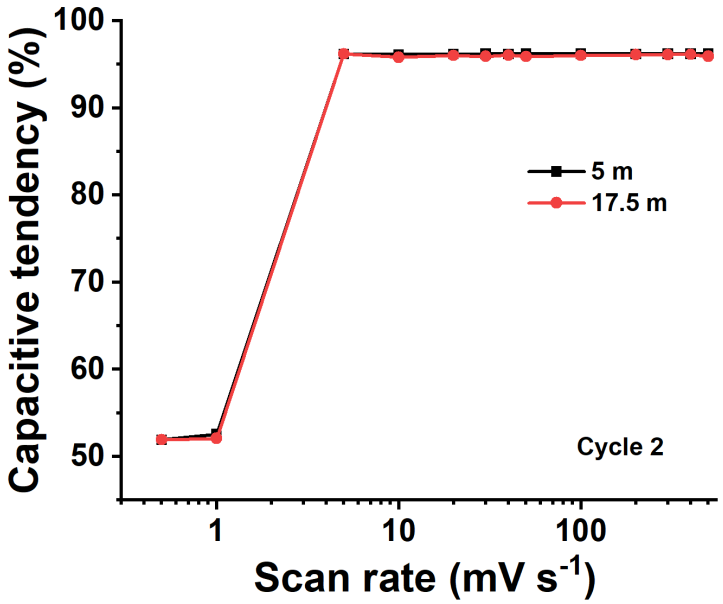

Figure S11: Analysis of the capacitive tendency of cyclic voltammograms of $V_4C_3T_z$ electrodes according to a *TB Robot* supervised machine learning tool[2,3] (See main text). The cyclic voltammograms were performed at 0.5 to 500 mV s^{-1} scan rate, 5 m and 17.5 m LiBr electrolytes and -0.7 to 0.7 V vs. Ag (5 m) and -0.7 to 0.8 V vs Ag (17.5 m) electrochemical windows according to Figure S15a,f.

S7 Cyclic voltammetry over cyclability tests

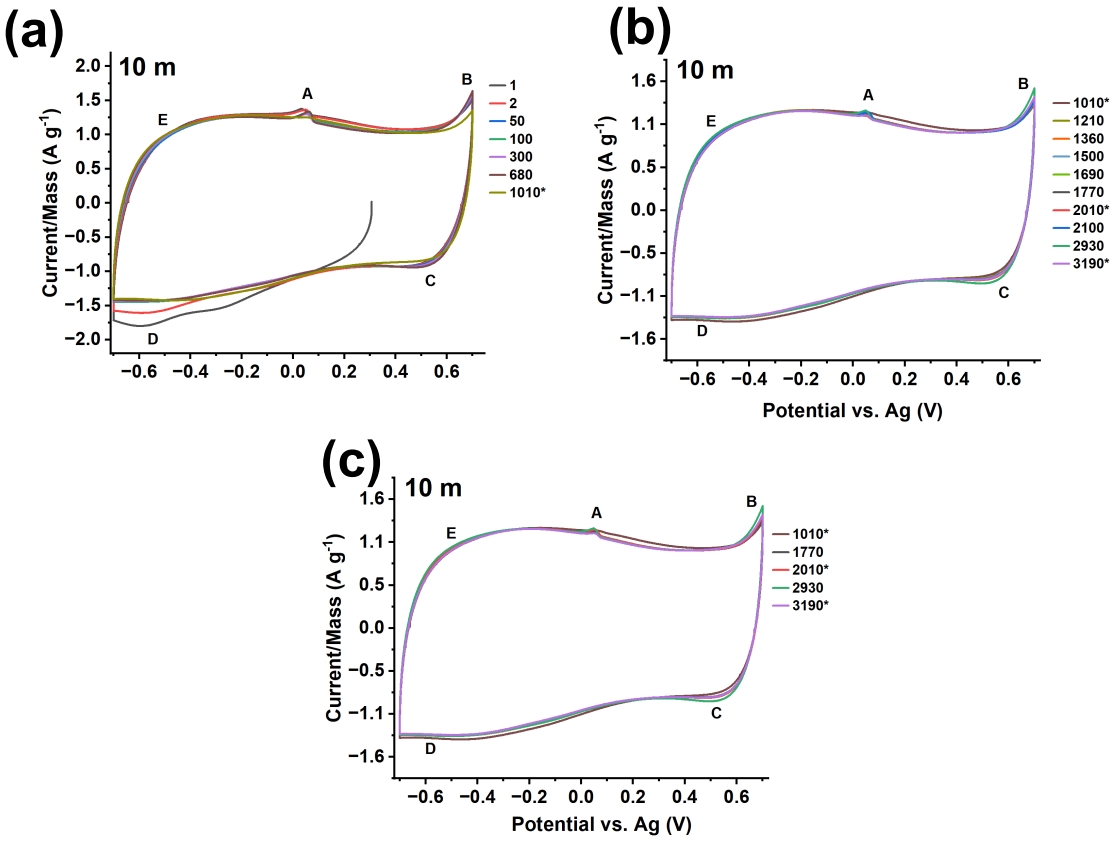

Figure S12: CVs of cyclability tests performed at 10 mV s^{-1} of $V_4C_3T_z$ film electrodes in a half cell set up, a -0.7 to 0.7 V vs. Ag electrochemical window and a 10 m LiBr electrolyte. (a-c) CVs number indicated in the legend. CVs performed just after separator and electrolyte change are indicated with an asterisk.

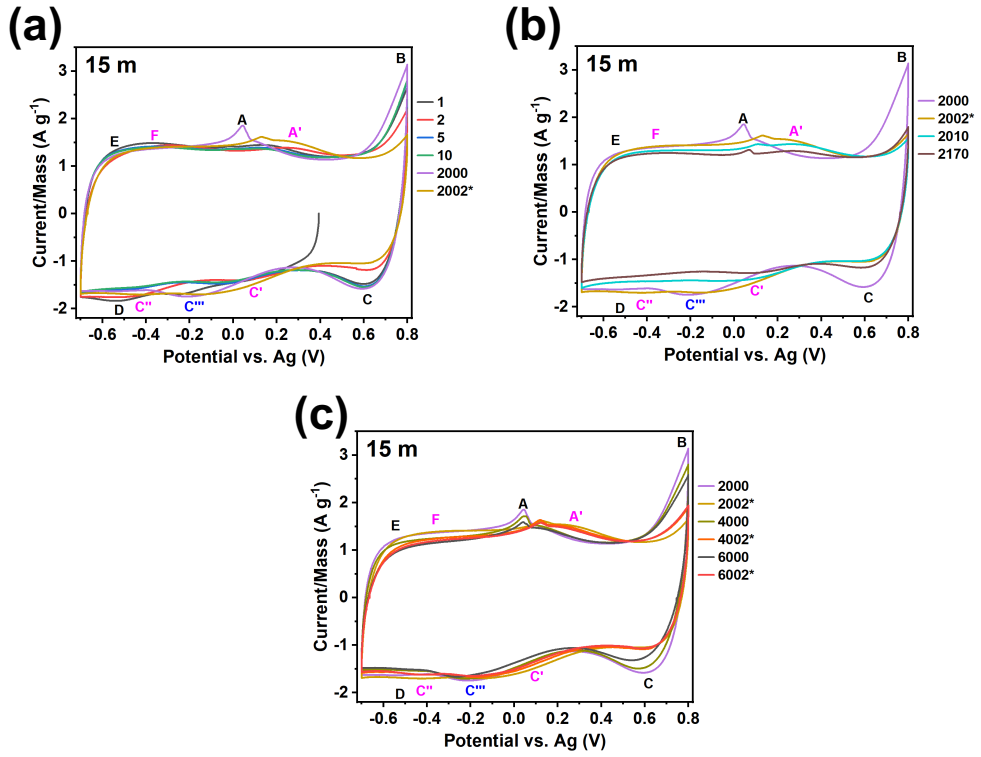

Figure S13: CVs of cyclability tests performed at 10 mV s^{-1} of $V_4C_3T_z$ film electrodes in a half cell set up, a -0.7 to 0.8 V vs. Ag electrochemical window and a 15 m LiBr electrolyte. (a-c) CVs number indicated in the legend. CVs performed just after separator and electrolyte change are indicated with an asterisk.

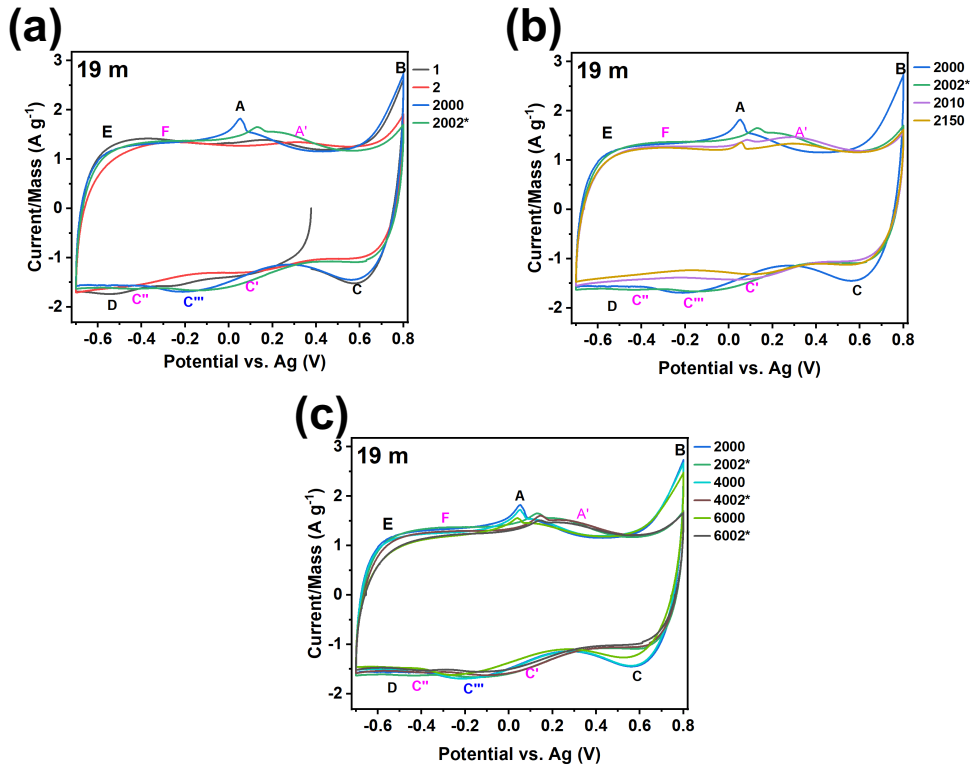

Figure S14: CVs of cyclability tests performed at 10 mV s^{-1} of $V_4C_3T_z$ film electrodes in a half cell set up, a -0.7 to 0.8 V vs. Ag electrochemical window and a 19 m LiBr electrolyte. (a-c) CVs number indicated in the legend. CVs performed just after separator and electrolyte change are indicated with an asterisk.

S8 Cyclic voltammetry over scan rates

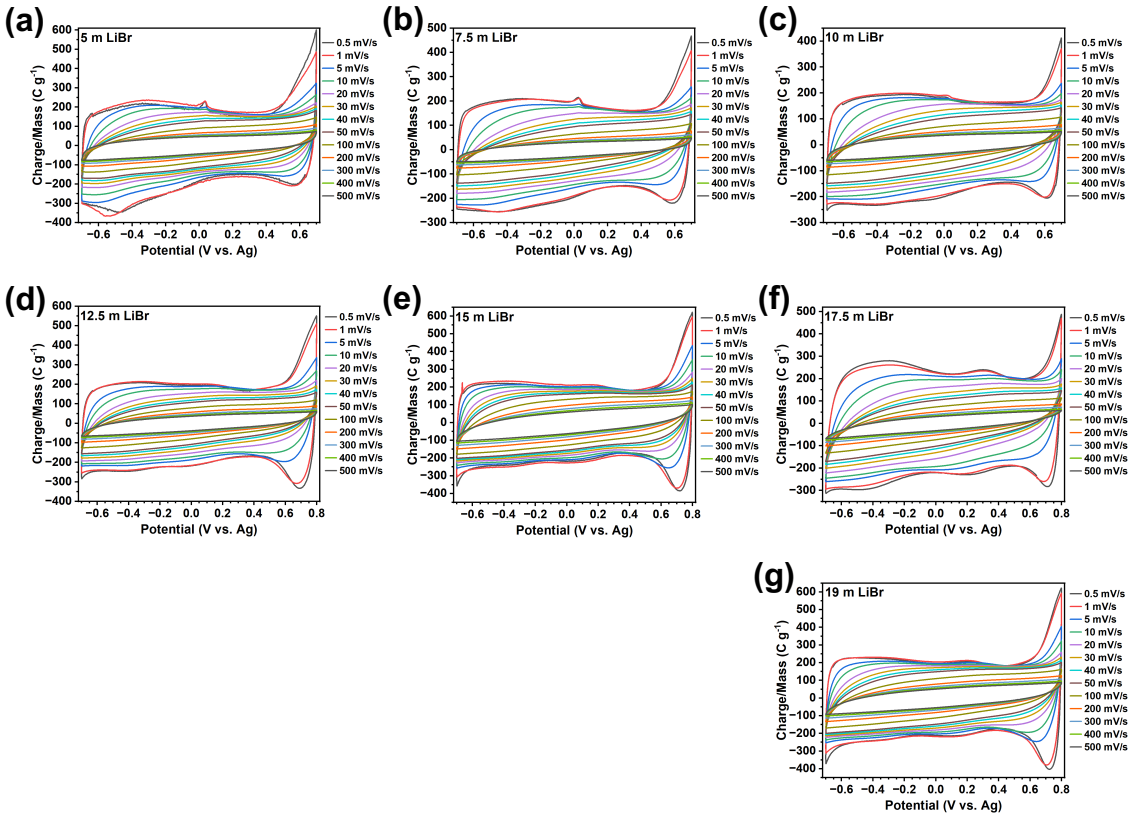

Figure S15: CVs at a range of scan rates for $V_4C_3T_z$ film electrodes in a half cell set up in (a) 5 m LiBr, (b) 7.5 m LiBr, (c) 10 m LiBr, (d) 12.5 m LiBr, (e) 15 m LiBr, (e) 17.5 m LiBr, and (e) 19 m LiBr.

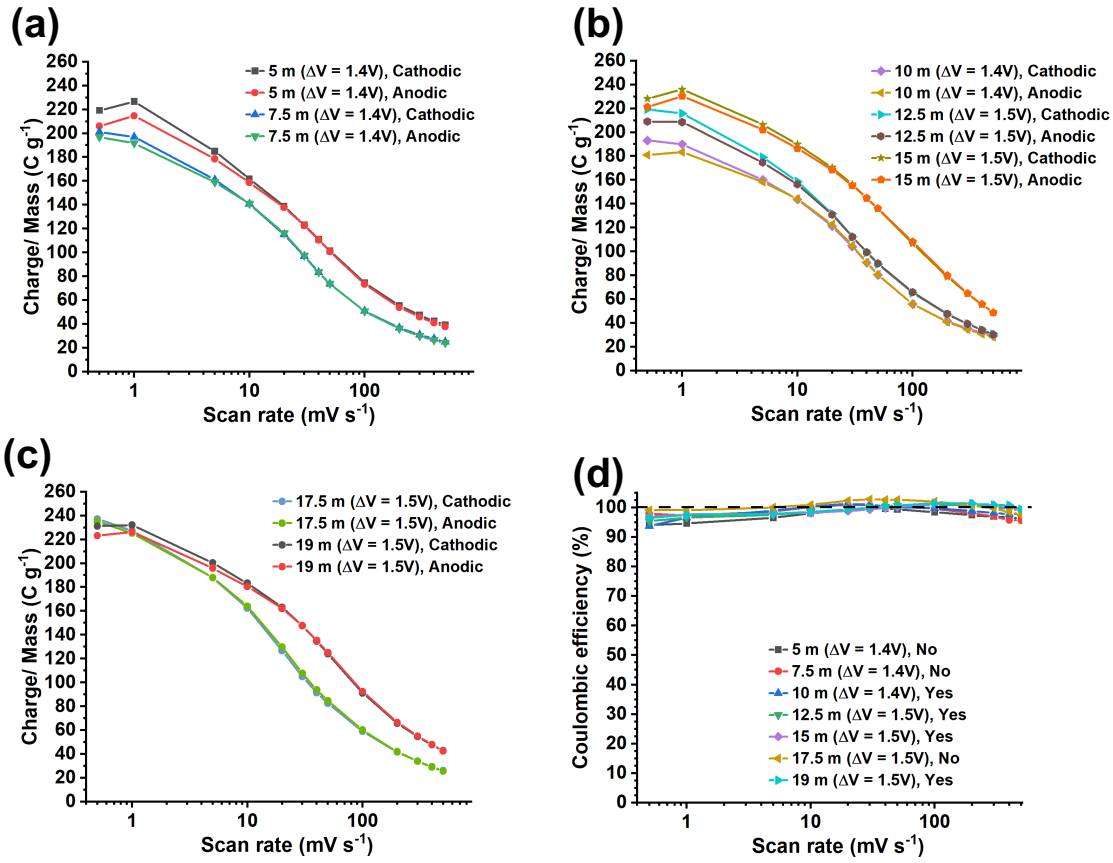

Figure S16: (a)-(c) Cathodic and anodic charge storage vs. scan rate curves for electrodes tested in 5 m to 19 m LiBr electrolytes, (d) the corresponding Coulombic efficiency curves. The notes "Yes" or "No" indicate whether the electrode underwent an activation procedure (step 6).

S9 EIS data

S9.1 EIS models elements

The EIS data was modeled with models 1 and 2 described in the main text (Figure 9). These models involve the following elements. The impedance of a generalized open circuit terminus Warburg element or blocked diffusion phenomena, Z_{W_o}, derived using reflective boundary conditions (described in the main text) is defined as:[4–6]

$$Z_{W_o} = R_W \frac{coth(i\omega T_W)^{0.5p}}{(i\omega T_W)^{0.5p}} \tag{S1}$$

where $i = \sqrt{-1}$ accounts for the imaginary component of a complex number, $\omega = 2\pi$f, is angular frequency (rad s^{-1}), where f is frequency (Hz), and $0 < 0.5p \leq 1$ is a constant that accounts for the frequency dispersion of the impedance at low frequency. Notice that in the *Zview* software, W-P = 0.5p. For p = 1 (no frequency dispersion):

$$R_W = \frac{RT\delta}{z^2F^2Ac_o^*D} \tag{S2}$$

is the resistance to diffusion (Ω), where R is the ideal gas constant (8.3143 J mol^{-1} K^{-1}), T is the temperature (K), δ is the diffusion length of the electrode (electrode thickness), z is the number of electrons released or consumed in a Faradaic process, according to Faraday charge transfer law, $F$is the Faraday constant (96,485 C mol^{-1}), A is the electrode area, c_o^* is the concentration of charge carriers in equilibrium (bulk) (mol cm^{-3}) and D is the diffusion coefficient (cm^2 s^{-1}). When p < 1, D should be replaced by a different parameter $\widehat{D}$ (cm^2 s^{-p}), which is defined as an anomalous diffusion parameter.[4]

The parameter T_W is the time constant to diffuse chemical species through a finite length medium:

$$T_W = \left(\frac{\delta^2}{\widehat{D}}\right)^{(1/p)} \tag{S3}$$

When p = 1, $\widehat{D}$ is D. A characteristic frequency is defined as $f_W = 1/(2\pi f)$ defined as the transition from the semi-infinite diffusion behavior (Z' = -Z") to the capacitive behavior when 60 % of the charge carriers have accumulated at the blocked interface.[4]

The anomalous diffusion coefficient $\widehat{D}$ can then be calculated as:

$$\widehat{D} = \frac{\delta^2}{T_W^p} \tag{S4}$$

S9.2 EIS data of electrodes tested in the 17.5 m and 5 m LiBr electrolytes

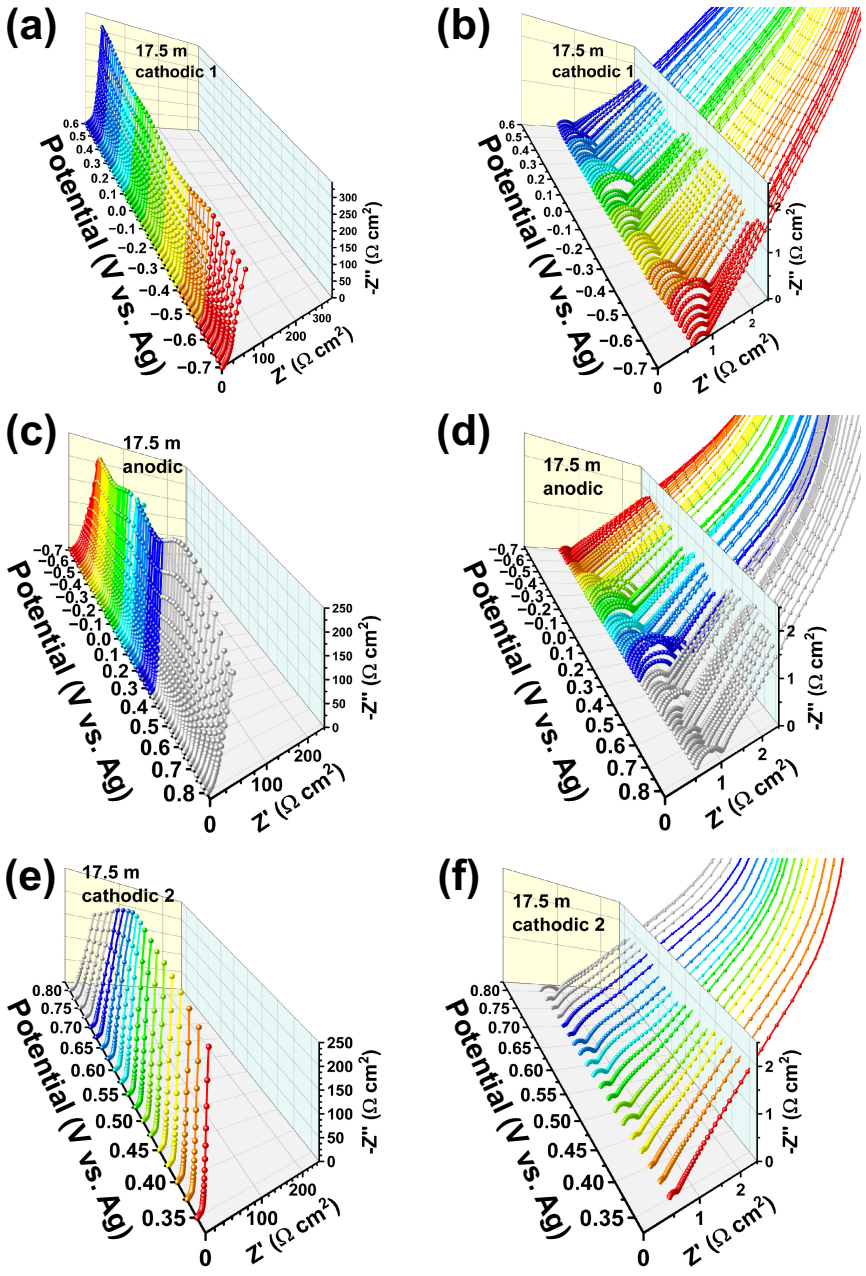

Figure S17: 3D Nyquist plots of the EIS data of the electrode tested in the 17.5 m LiBr electrolyte. (a),(b) cathodic scan 1, (c),(d) anodic scan, (e),(f) cathodic scan 2. (b),(d) and (f) are insets of (a),(c) and (e).

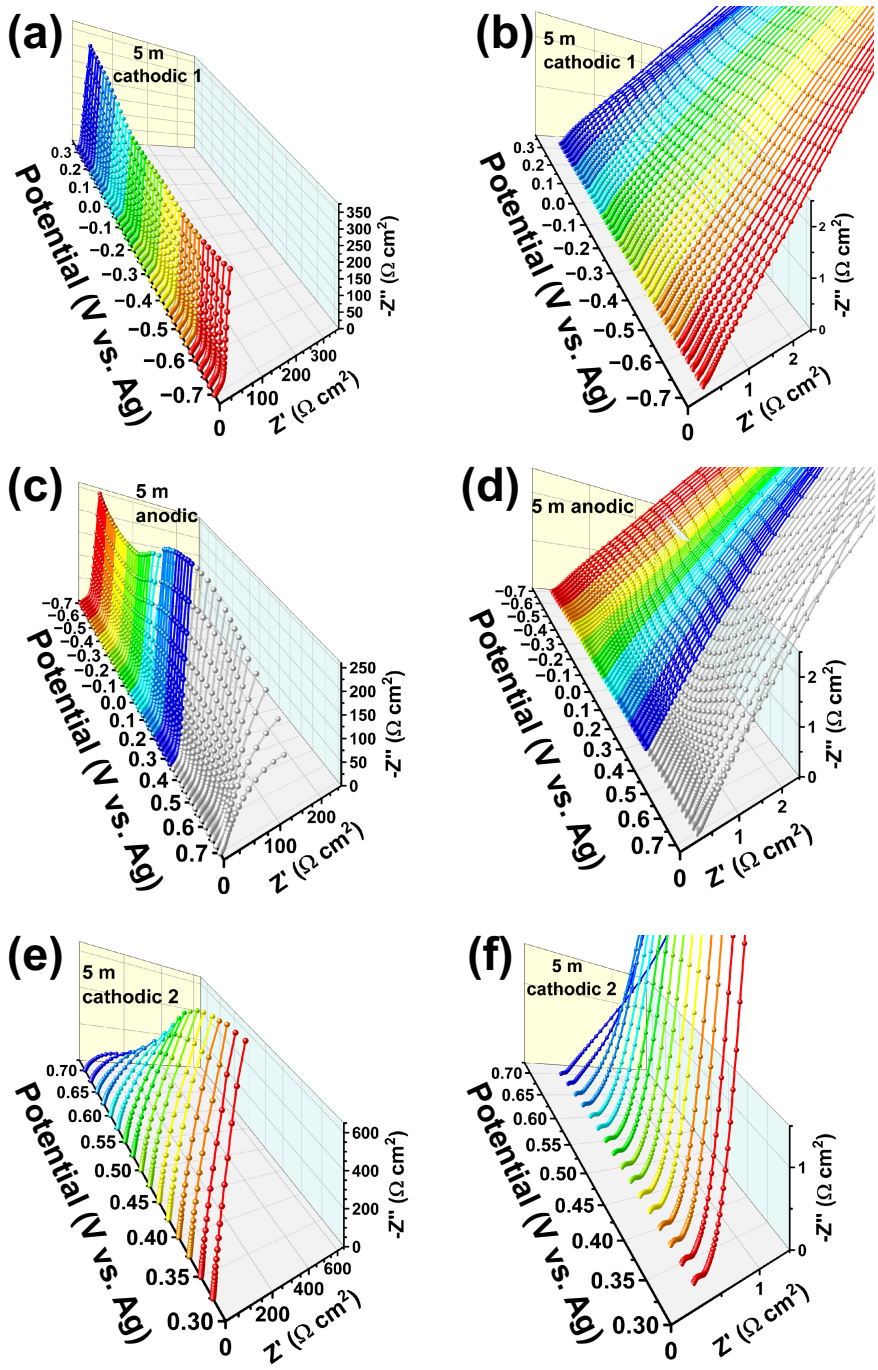

Figure S18: 3D Nyquist plots of the EIS data of the electrode tested in the 5 m LiBr electrolyte. (a),(b) cathodic scan 1, (c),(d) anodic scan, (e),(f) cathodic scan 2. (b),(d) and (f) are insets of (a),(c) and (e).

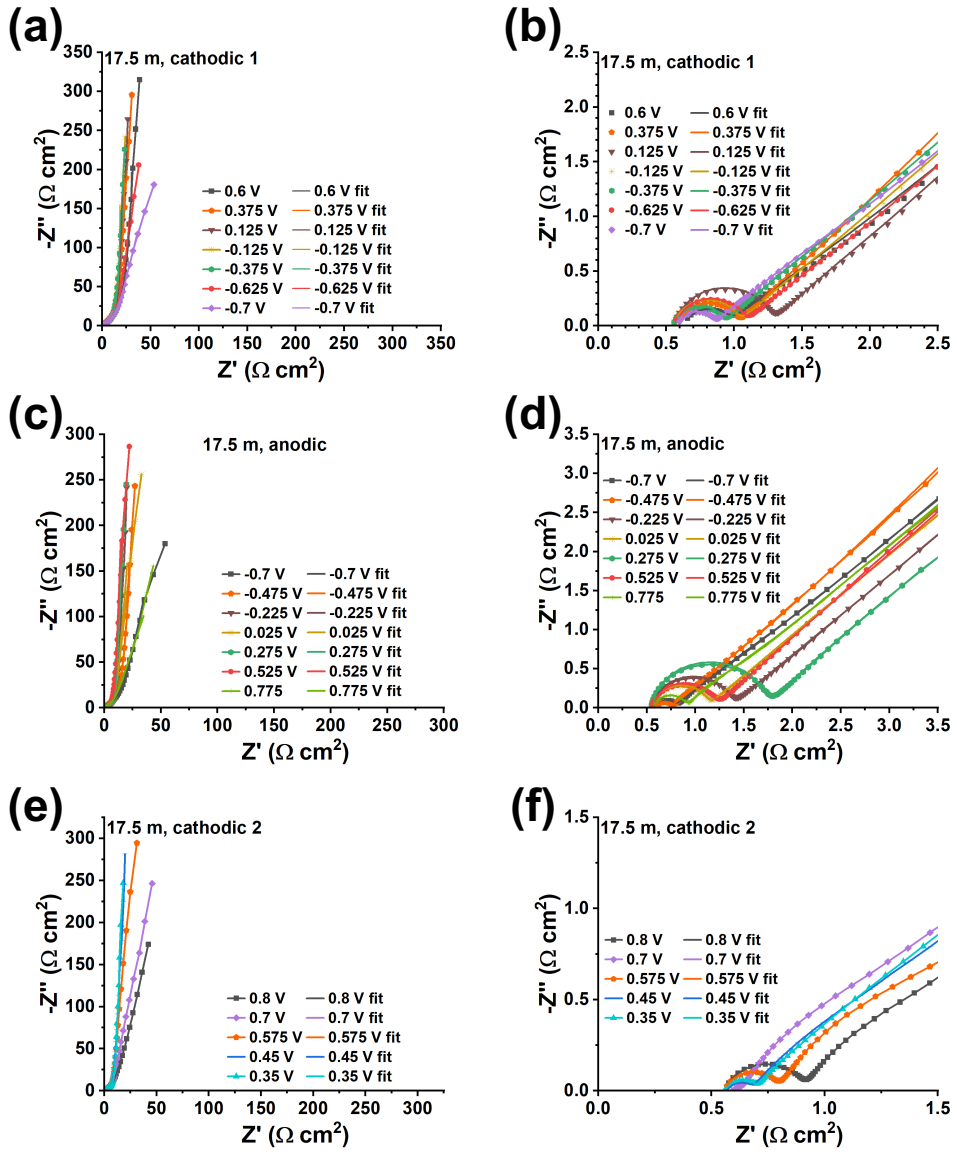

Figure S19: 2D Nyquist plots of selected EIS data of the electrode tested in the 17.5 m LiBr electrolyte and corresponding data fit using model 1. (a),(b) cathodic scan 1, (c),(d) anodic scan, (e),(f) cathodic scan 2. (b),(d) and (f) are insets of (a),(c) and (e).

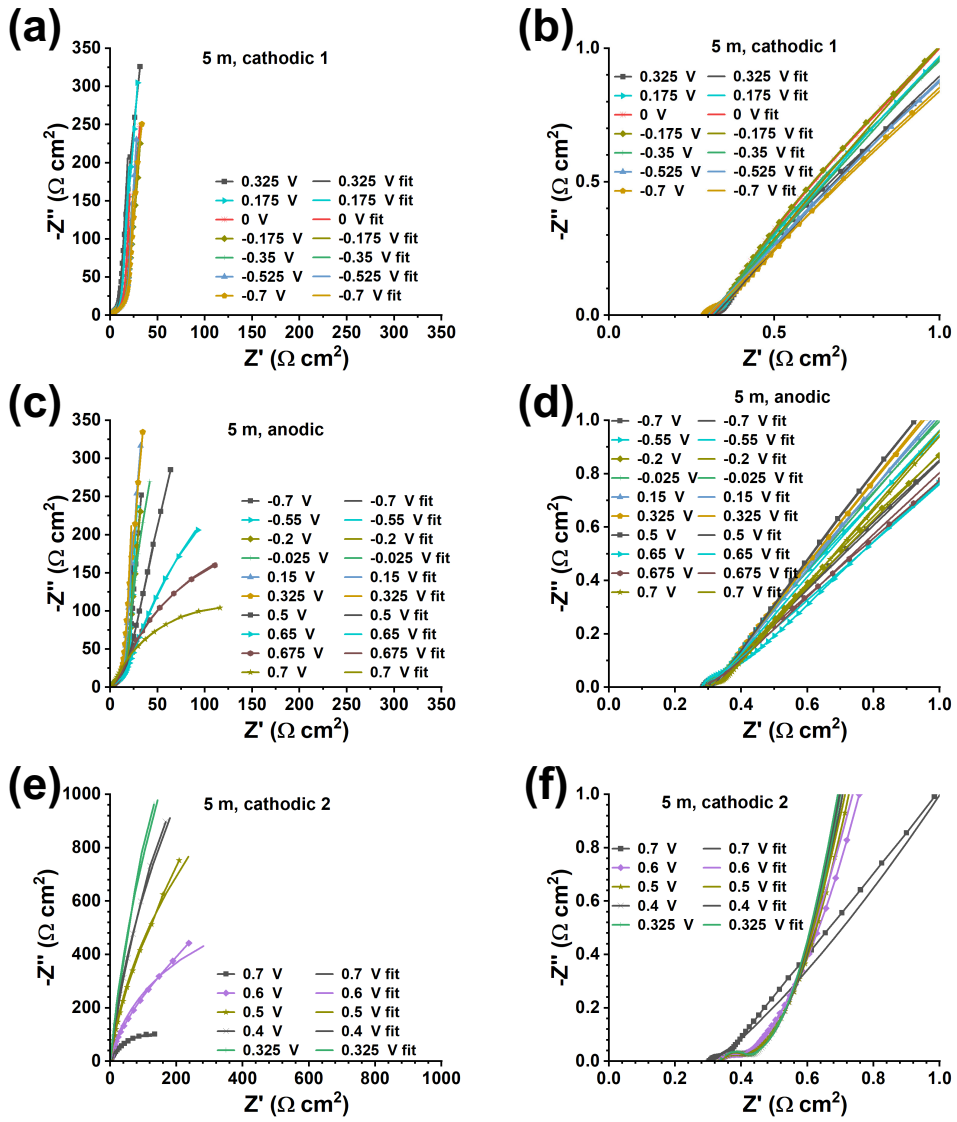

Figure S20: 2D Nyquist plots of selected EIS data of the electrode tested in the 5 m LiBr electrolyte and corresponding data fit. (a),(b) cathodic scan 1 (modeled with model 2), (c),(d) anodic scan (modeled using model 2 from -0.7 V to 0.625 V and model 1 from 0.65 to 0.7 V), (e),(f) cathodic scan 2 (modeled using model 1). (b),(d) and (f) are insets of (a),(c) and (e).

S9.3 Calculation of diffusion coefficients

Anomalous diffusion coefficients were calculated according to the parameters derived from the data fit using models 1 and 2 (Figure 9) and Equation S4. According to a p $\approx$ 1 value, the diffusion coefficient was a standard diffusion coefficient.

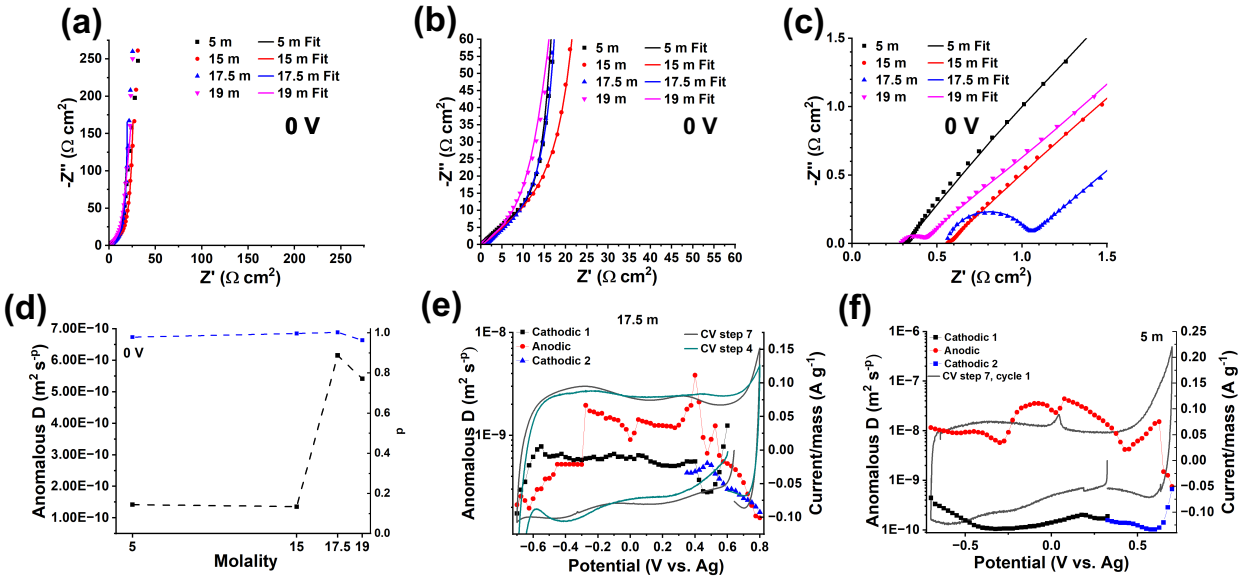

Figure S21: (a)-(c) Nyquist plots of EIS data of electrodes tested in 5, 15, 17.5 and 19 m LiBr electrolytes and polarized at 0 V during the cathodic scan 1, along with data fit obtained using models 2 (5 m and 15 m LiBr EIS data) and model 1 (17.5 m and 19 m LiBr EIS data), (d) corresponding calculated diffusion coefficients (Equation S4) vs. electrolyte concentration curve, (e) calculated diffusion coefficients vs. polarization potential curves of the experiment using the 17.5 m LiBr electrolyte, as determined according to the fit to model 1, and CVs at 0.5 mV s^{-1} (cycle 1) for steps 4 and 7 of the experiment in Figure 3, (f) calculated diffusion coefficients vs. polarization potential curves of the experiment at 5 m LiBr electrolyte, as determined by fitting model 2 (cathodic scan 1), model 2 (anodic scan from -0.7 V to 0.625 V) and model 1 (anodic scan from 0.65 V to 0.7 V and cathodic scan 2), and CVs at 0.5 mV s^{-1} (cycle 1) for step 7 of the standard testing sequence (with no activation, step 6).

S9.4 Capacitive response

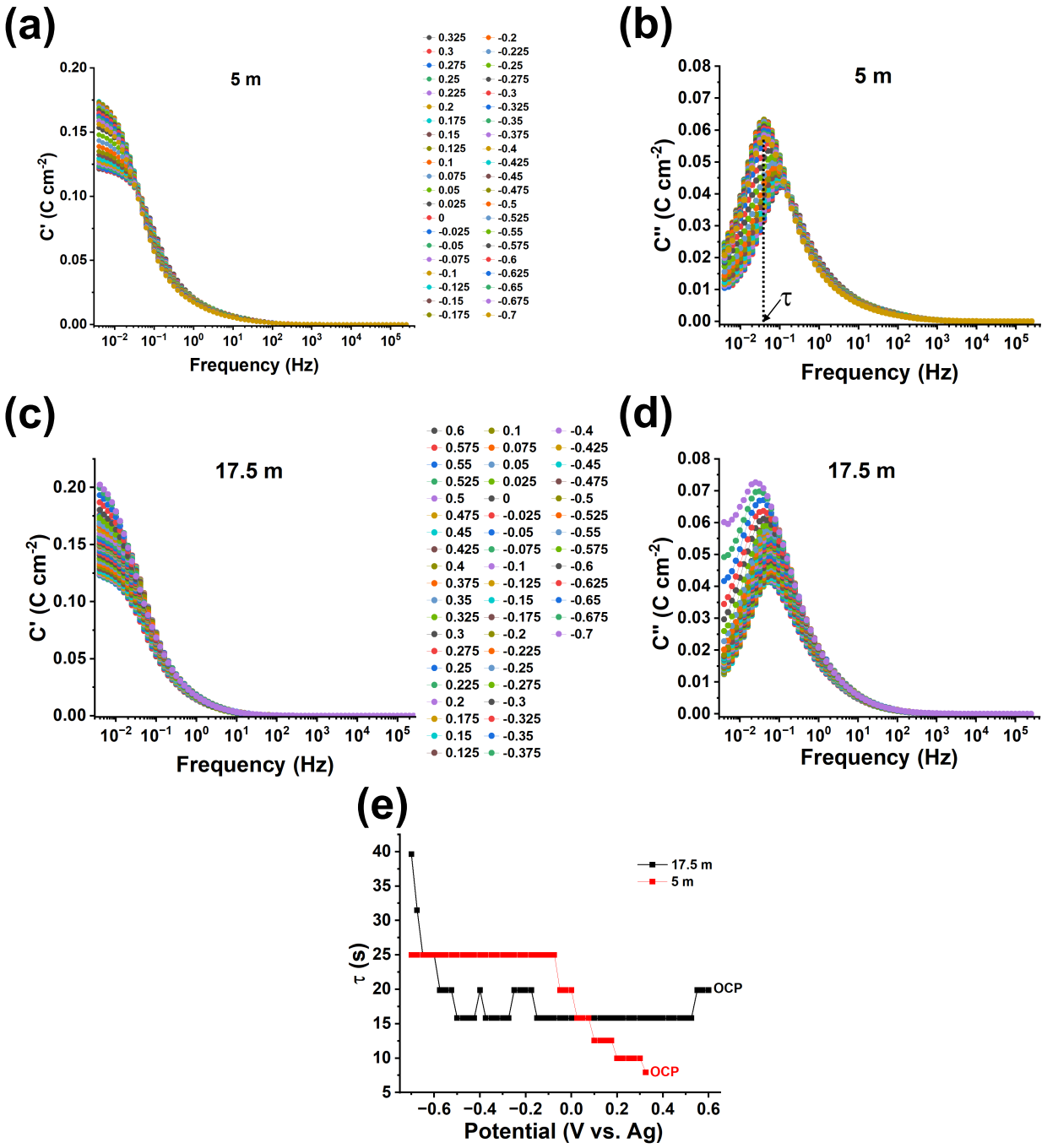

Figure S22: Capacitance and capacitive response of electrodes tested in 5 m and 17.5 m LiBr electrolytes using SPEIS measurements, cathodic scan 1. (a),(c) Real (C') and (b),(d) imaginary (C") components of the capacitance vs. frequency curves of electrodes tested in (a),(b) 5 m and (c),(d) 17.5 m electrolytes, (d) corresponding capacitive response (τ) vs frequency curves. The main text describes calculations.

References

(1) Mendoza-Sánchez, B.; Ladole, A. H.; Samperio-Niembro, E.; Mangold, S.; Knapp, M.; Tseng, E. N.; Persson, P. O. ; Douard, C.; Shuck, C. E.; Brousse, T. On the atomic structure of monolayer $V_4C_3T_z$ and the study of charge storage processes in an acidic electrolyte using SPEIS and in-situ X-ray absorption spectroscopy. *Energy Storage Materials* **2024**, *71*, 103566.

(2) 2024; `http://supercapacitor-battery-artificialintelligence.vistec.ac.th/CV`.

(3) Deebansok, S.; Deng, J.; Le Calvez, E.; Zhu, Y.; Crosnier, O.; Brousse, T.; Fontaine, O. Capacitive tendency concept alongside supervised machine-learning toward classifying electrochemical behavior of battery and pseudocapacitor materials. *Nature Communications* **2024**, *15*, 1133.

(4) Cruz-Manzo, S.; Greenwood, P. Frequency Transition from Diffusion to Capacitive Response in the Blocked-Diffusion Warburg Impedance for EIS Analysis in Modern Batteries. *Journal of The Electrochemical Society* **2020**, *167*, 140507.

(5) Cruz-Manzo, S.; Greenwood, P. Blocked-Diffusion with Frequency Dispersion for Study of EIS in NiMH Batteries. *Journal of The Electrochemical Society* **2019**, *166*, A1176.

(6) Cruz-Manzo, S.; Greenwood, P.; Chen, R. An Impedance Model for EIS Analysis of Nickel Metal Hydride Batteries. *Journal of The Electrochemical Society* **2017**, *164*, A1446.